Int J Adv Manuf Technol (2016) 82:1921–1931
DOI 10.1007/s00170-015-7507-2

ORIGINAL ARTICLE

Development of hybrid process for double-side flexible printed circuit boards using roll-to-roll gravure printing, via-hole printing, and electroless plating

Janghoon Park[1] · **Jongsu Lee**[1] · **Sungsik Park**[1] · **Kee-Hyun Shin**[2,3] · **Dongjin Lee**[2,3]

Received: 23 February 2015 / Accepted: 26 June 2015 / Published online: 14 July 2015

Abstract A hybrid process including roll-to-roll (R2R) gravure printing, via-hole printing, and electroless plating was investigated for the creation of a double-side flexible printed circuit board (FPCB). A R2R gravure process with an Ag seed layer that includes front- and back-side printing with a polyimide film at the center was investigated. The gravure-printed Ag pattern was laser drilled for high accuracy. A via hole was filled with a low-viscosity Ag ink using the drop-casting method. In addition, an electroless Cu plating process was performed to increase the conductivity of the printed circuit. The interconnection performance was confirmed from the resistance values obtained using a feed-through test and microscopic images. To evaluate the reliability of the FPCB, a cyclic bending motion test was performed; stable electrical performance was observed even after 400,000 cycles. The results obtained in this study suggest that the proposed hybrid process for double-side FPCBs is viable for a mass production system.

Keywords Flexible printed circuit board · Roll-to-roll · Printed electronics · Double-side printing · Via hole · Reliability test

✉ Dongjin Lee
djlee@konkuk.ac.kr

[1] Department of Mechanical Design and Production Engineering, Konkuk University, 120 Neungdong-ro, Gwangjin-gu, Seoul 143-701, Korea

[2] School of Mechanical Engineering, Konkuk University, 120 Neungdong-ro, Gwangjin-gu, Seoul 143-701, Korea

[3] Flexible Display Roll-to-Roll Research Center, Konkuk University, 120 Neungdong-ro, Gwangjin-gu, Seoul 143-701, Korea

1 Introduction

Printed electronics has been spotlighted as an eco-friendly, cost-effective, and scalable technology. Unlike batch-processed applications based on chemical etching, printed electronics use a multilayer printing method in which each layer is successively deposited on a substrate. Examples of such devices include capacitors, thin-film transistors (TFTs), organic photovoltaics (OPVs), and organic light-emitting diodes (OLEDs). Recent studies have focused on developing processes to improve the scale (minimization), performance, and surface morphologies of multilayer printed devices [1–3].

Thus far, studies have investigated printed applications that use various printing techniques. Printing techniques have advantages and disadvantages in the mass productivity, resolution, and accessibility of their patterning, which is related to the process, properties of ink, and substrates. Inkjet printing [4–7], screen printing [8–10], and slot die coating [11–14] were adopted as process methods according to the requirements of the target device. However, these techniques have limitations in their large-area printing capabilities, fine-line pattering, and flexibility of patterning, respectively.

A promising alternative is gravure printing, on which we focused in this study. Gravure printing techniques are used for many applications such as TFTs, OPVs, OLEDs, and radio-frequency identification (RFID) tags [15–18]. Gravure printing methods can produce printed electronic devices with high processing speeds and permit various pattern designs, fine lines, and large-area printing. Gravure printing is also appropriate for roll-to-roll (R2R) continuous systems, a next-generation process in the printed electronics industry. In gravure printing processes with R2R systems, it is necessary to consider the mechanical (operating tension and speed) and chemical (viscosity and surface tension of ink) parameters that affect factors such as the thickness and roughness of the

printed pattern [19]. Researchers have already investigated these issues, and a mathematical model has been developed to predict the surface profile using statistical analysis [20]. The optimal process parameters for factors such as ink viscosity and printing speed have also been investigated [15]. Recently, studies have investigated stable and unstable regions of several parameters in R2R gravure printing. Furthermore, to minimize the printing scale and improve important process parameters, guidelines have been suggested for optimizing the R2R gravure printing process [21, 22].

Most of the abovementioned existing processes use a sequential deposition method called multilayer printing. Traditional mass-produced integrated circuits (IC) consist of single- or a double-side flexible printed circuit boards (FPCBs) based on multilayer printing. As shown in Fig. 1, FPCBs can be categorized as one-side FPCBs containing several conductive layers, with a dielectric layer between one side of the substrate (Fig. 1a) and an individual conductive layer on each side of substrate, interconnected by a via hole (also called a through hole) (Fig. 1b).

Double-side-type FPCBs such as the one depicted in Fig. 1b are most frequently fabricated by the screen and inkjet printing methods. As mentioned above, double-side printed patterns include a via hole to electrically connect the front and the back layers; this is an important technology for not only double-side printing but also interconnection techniques for finished products [10, 23–26]. Various printing methods can be used depending on the layer characteristics. Such systems are called *hybrid processes*, and integration of the

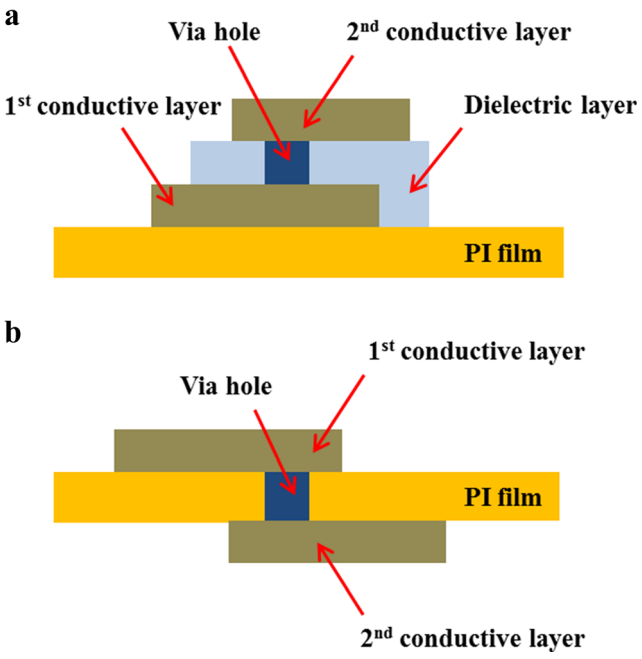

Fig. 1 Design of double-side FPCB attainable in printed electronics: **a** two conductive layers with dielectric layer between on one side of PI film and **b** individual conductive layer on each side of PI film with through hole

printing methods is necessary to maximize the efficiency of the products [27, 28]. Furthermore, it is necessary to adopt the Cu plating process to improve the electrical performance of a FPCB in the presence of Ag material limitations [29, 30].

In the present work, the hybrid printing and interconnection processes were introduced. These processes include the printing and plating processes. In the section about printing, a R2R gravure printing process was used to fabricate the double-side printed Ag seed layer. The hole was made by laser drilling, and the via hole was made with Ag ink by the drop-casting method using micropipettes. In the section that addresses plating, an electroless Cu plating method was used to enhance the electrical performance. The printability and functionality of the fabricated double-side FPCB was confirmed through microscopic and electrical measurements. The final product obtained through this experiment was verified, via a reliability test, to have high stability. This experiment was conducted using a large-scale R2R system using double-side seed layer printing that can check the required properties during mass production. Furthermore, via-hole printing and the Cu electroless plating process could be extended to the R2R process level and utilized in various electronic applications as a preliminary study.

2 Materials and method

2.1 Experimental setup

The R2R gravure printing system (Sung An Machinery Co., Korea) in Fig. 2a consists of unwinding, infeeding, preheating, printing (direct gravure), drying (hot air), lateral guiding, outfeeding, cooling, and rewinding sections. This R2R system had a maximum operating speed of 50 m/min and an operating tension limit of 200 N. The register control unit is divided into machine directional (MD) and cross-machine directional (CMD) alignments. The MD register was manually controlled using a roll-phase controller (Bosch Rexroth Co., Germany), and the CMD register was maintained in a specific position using a lateral web guider (FIFE Co., USA).

The substrate and printing materials used are presented in Table 1. Polyimide (PI) has been widely adopted in FPCB processes and was used as the substrate owing to its excellent thermal robustness compared to polyethylene terephthalate (PET) film. With thermally stable PI film, a high-temperature curing condition can be adopted to achieve high conductivity. In R2R gravure printing, doctoring defects, which often occur when using Ag nanoparticle ink, significantly affect the device performance. For that reason, Ag flake gravure paste (purchased from Fine Paste Co.), which has a large particle size, was used as the conductive layer to prevent doctoring defects [22]. In addition, Ag nanoparticle ink

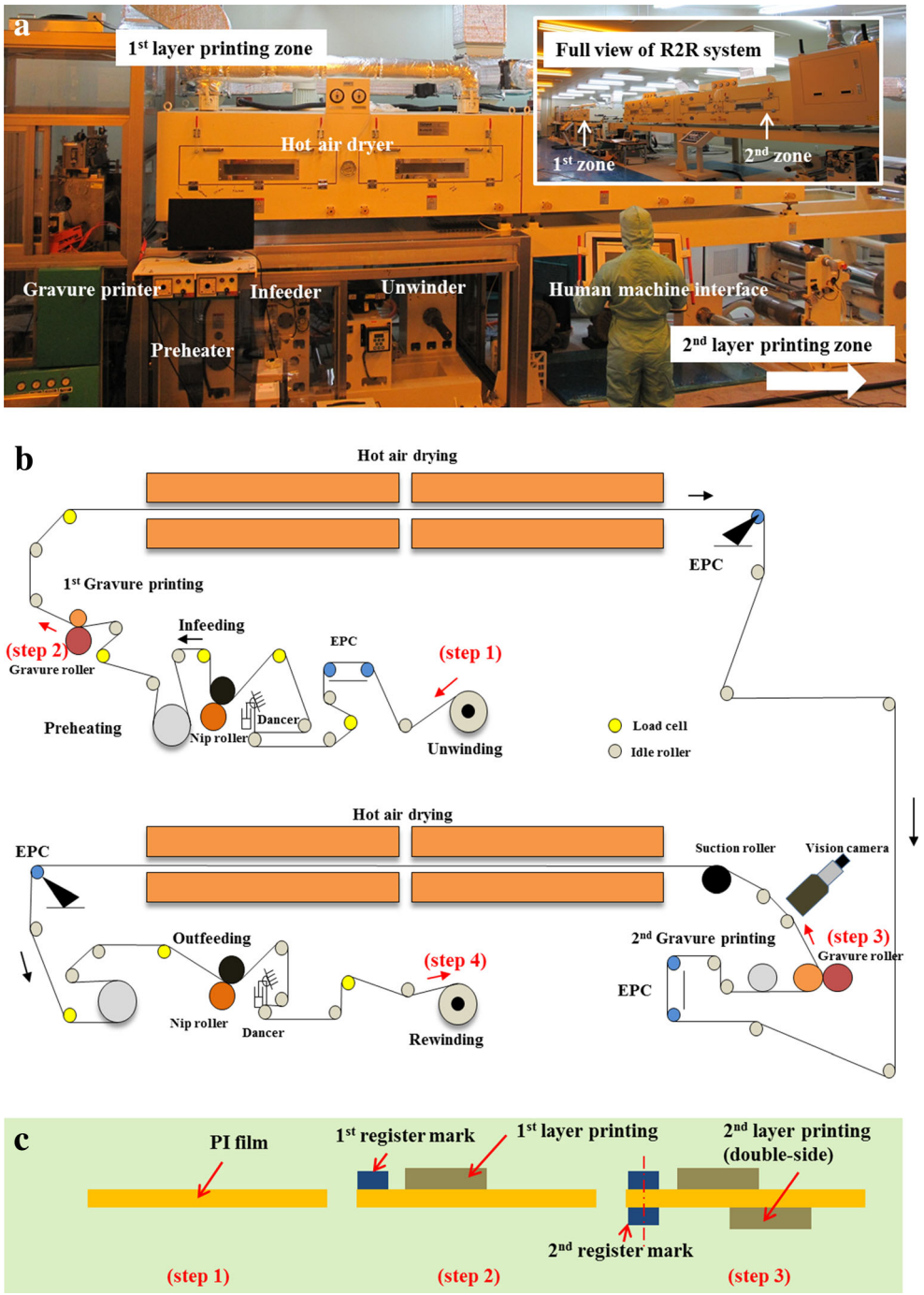

Fig. 2 FPCB fabrication process using an R2R gravure printing system: **a** industrial-scale R2R gravure printing module, **b** schematic diagram of the R2R system used in this study, and **c** cross-sectional view of the FPCB at each position in **b**

(Advanced Nano Products Co., Korea) was used for the filling process (via hole) for the laser-drilled holes.

The process conditions for the R2R printing and via-hole filling are shown in Table 2. In the R2R gravure printing process, the operating speed was selected by considering the minimum drying time and drying chamber length for the printed pattern. In addition, the operating tension was set to a low value to prevent wrinkles and air entrainment. Nip pressure and doctoring pressure are critical parameters that affect the printability (ink transfer) of the gravure pattern. In detail, the nip and doctoring pressure determine the filling, setting, and printing phase on the gravure cell to the substrate. The optimized value of pressure was selected by the experimental procedure followed in previous work [31, 22]. After finishing the gravure printing process, the wound film was sampled by a slitting process and was laser-drilled at the interconnection point. The drilled hole was filled with Ag ink. After ink filling was achieved using micropipettes, infrared (IR) was used to dry the via hole. The Cu plating process has been adopted industrially for the fabrication of FPCBs. During this plating

Table 1 Substrate and printing materials

Material	Parameter	Unit	Value
PI film	Width	mm	300
	Thickness	μm	25
Ag flake (pattern)	Particle size	μm	1.93
	Viscosity	cP	3423
	Thixotropy	–	4.2
Ag nanoparticle (via hole)	Solid contents	wt%	30
	Viscosity	cP	16.8
	Surface tension	dyn/cm	35–38

step, the Ag double-side printed circuit is covered with a Cu layer. In the plating process, each step can experience defects such as delamination, bubbles, and nonuniformity. The mixing ratio of plating materials and plating times should be optimized to improve the plating quality. The plating process consists of several steps, and the optimized conditions are listed in Table 3.

The thickness, surface morphology, and functionality of the printed patterns were characterized with an interferometer (NV-2000, Nano System Co., Korea) and atomic force microscope (AFM, XE-1000, PSIA Co., Korea), optical microscope (HVM0850D, E-flex Co., Korea), and digital multimeter (Fluke Co., USA), respectively. Moreover, scanning electron microscope (SEM) images and energy-dispersive spectroscopy (EDS) data were obtained by using a field emission SEM (S-4800, Hitachi, Japan).

The FPCB was subjected to a cyclic bending test to evaluate its reliability. The endpoint of the sample was fixed, and a Cu tape was attached to it to measure the resistance in real time by using SourceMeter (Kiethley, Tektronix Co., USA). The bending cycles had radii of 5 and 12 mm on the near coil pattern and via hole, respectively. The number of cycles was determined depending on the final product [32–36]. In this case, up to 400,000 cycles were performed to confirm the mechanical stability of the FPCB.

In addition, the coil-printed and interconnected FPCB was demonstrated as an RFID antenna device. A function generator (8116A, Hewlett-Packard, USA) and oscilloscope (DS1052E, RIGOL Co., USA) were used to measure the resonance frequency of the circuit.

Table 2 Process parameters of the printing step

Parameter	Unit	Value
Operating speed	m/min	5
Operating tension	N	10
Drying temperature	°C	150
Drying time	min	2 (pattern), 10 (via hole)
Nip pressure	MPa	0.5
Doctor pressure	MPa	0.5

2.2 Double-side printing

A novel printing logic was used to produce a double-side FPCB with R2R gravure printing, as shown in Fig. 2 [37]. Traditional R2R gravure printing processes include a sequence of multiple layers added from the substrate to the top layer with conductive and dielectric materials, as shown in Fig. 1a. By contrast, the proposed technique uses a double-side gravure printing process after the first layer is printed, as shown in Fig. 2b, c. PI film is transported from the unwinder to the first printing section (step 1), the first layer is printed (step 2), and then, the printed pattern is passed through the drying section and transported to the second printing module. Back-side printing is performed in the second printing section using direct gravure printing in alignment with the first printed pattern (step 3). Register control is a key issue in step 3; the MD register control is adjusted using the manual phase control of the second printing roller, and the CMD register is controlled using a lateral guide system. Double-side printed Ag seed patterns are then passed through the drying section and are finally rewound in the rewinding section (step 4).

2.3 Laser drilling and interconnection

Figure 3 shows the drilling and interconnection process. To begin the laser drilling and interconnection of the board halves, a slitting process for the double-side, printed wound roll was conducted, as shown in Fig. 3a. A sheet-type sampled film was drilled to a specific point using a laser process (Fig. 3b). Existing screen-printing processes were mainly used for the filling mechanism that extruded paste from the squeezed mesh [10]. Another study investigated via drilling by laser processing and confirmed the via-filling performance using inkjet printing [24]. Via filling of a 30–60-μm diameter has been achieved [27]. In this experiment, we used previous studies of practical applications for the interconnection of the sampled sheet. The drop method using micropipettes was selected. First, the double-side printed pattern was drilled, and a drop of low-viscosity Ag ink was applied to the drilled hole. If the droplet was located at a high position relative to the substrate, a defect would occur as the ink spread out (surface tension 35–38 dyn/cm), creating a short circuit in the printed pattern. Therefore, the ink was swept into the drilled hole naturally. The relevant capillary force is affected by proximal wall surfaces as well as the ink viscosity, as shown in Fig. 3c. After Ag ink was dropped, the IR dryer evaporated the solvent in the via hole, and there could be a scooped surface present around the hole owing to a coffee stain effect. The rand area and via hole were formed by the described ink drop process, and they were interconnected by the two rand patterns (upside

Table 3 Electroless Cu plating process steps and conditions

Process step (time)	Material	Combination
Neutral degreasing (5 min)	DI water	95.6 % (956 ml)
	Triethanolamine ($C_6H_{15}NO_3$)	4.4 % (44 ml)
Hot-water rinse (1 min)	DI water	100 % (1 l)
Pre-dip (1 min)	DI water	99 % (989 ml)
	Sulfuric acid (H_2SO_4)	1 % (10 ml)
Activator (3 min)	DI water	75 % (750 ml)
	Palladium sulfate ($PdSO_4$)	25 % (250 ml)
Cleaning (1 min)	DI water	–
Cu plating (30 min)	DI water	85.23 % (852 ml)
	Ethylene diamine tetra 2-propanol ($C_{14}H_{32}N_2O_4$)	9.9 % (99 ml)
	Dipyridyl-sodium [(C5H4N)-(C5H4N)]	0.3 % (3 ml)
	Sodium hydroxide (NaOH)	3.7 % (37 ml)
	Formaldehyde (CH_2O)	0.87 % (8.7 ml)
Cleaning (1 min)	DI water	–

and downside) and the surface of the hole. It is difficult to form a connection between double-side patterns without rand patterns. Hence, the ink drop process was performed two times to ensure that a rand pattern was formed, as shown in Fig. 3d. Figure 3e shows the additional Cu plating process that was adopted to reduce the resistance of the printed line. To

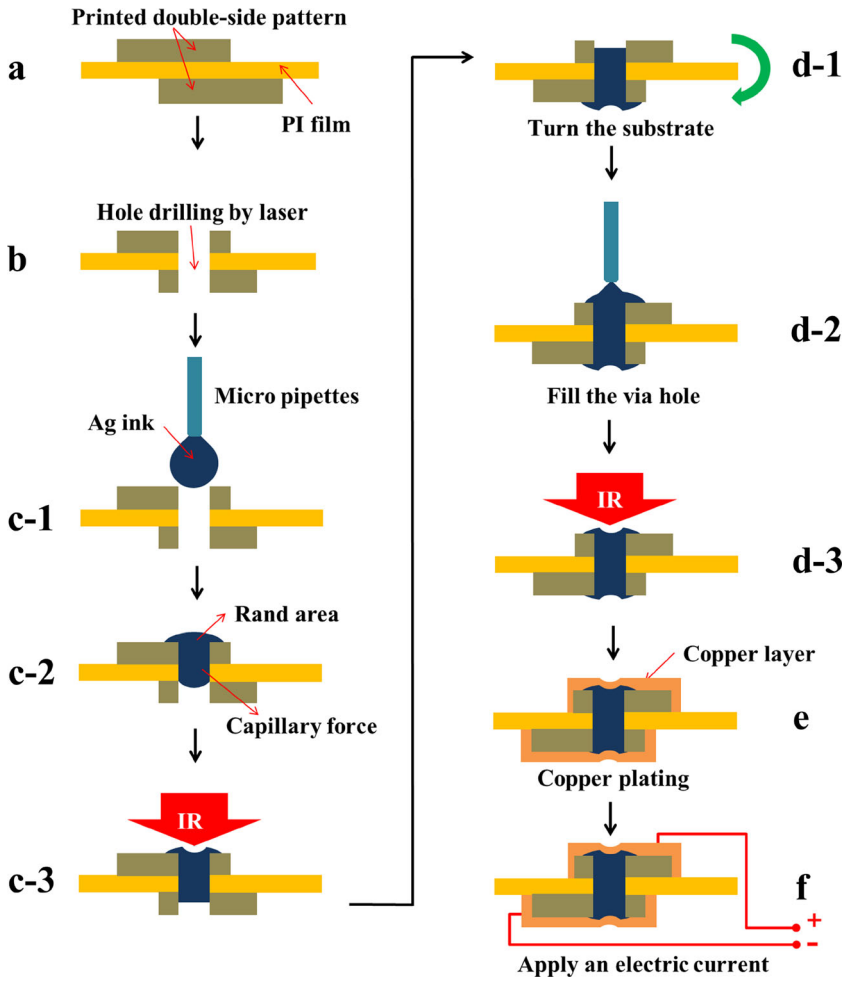

Fig. 3 Via-hole interconnection process: **a** printed double-side patterns using the R2R gravure process, **b** hole formation using a laser-drilling process, **c** Ag ink filling using capillary force, followed by an infrared drying process, (**d**) back-side ink filling and drying, **e** Cu plating, and **f** testing setup for interconnection performance

confirm the electrical performance, an electric current was applied to both rand areas after the interconnection process was completed, as shown in Fig. 3f.

3 Result and discussion

R2R gravure-printing processing was conducted using a computer-integrated, large-scale system that included web transport, printing, drying, and winding sections. Figure 4 shows the PI-film-based continuous printing process and its results. Figure 4a shows the rewind process of R2R gravure-printed double-side patterns. The final product of the gravure printing, consisting of two layers of patterns, is shown in Fig. 4b. Seven hundred-micrometer coil patterns were printed, for a total length of 1017.1 m on the front side, with a rectangular bridge pattern printed on the back side of the PI substrate. Figure 4c shows the double-side printing performance between PI substrates with precisely adjusted front- and back-side patterns. As mentioned earlier, register control was the most significant parameter in this experiment. Register errors caused misalignments in the via-drilling position. The PI film has good thermal stability that works better in controlling the tension of the web; web fluctuations are less prevalent relative to those in the case of PET films [38]. However, wrinkle phenomena occurred because of the thin substrate. FIFE guides were used to control the lateral position, and the operating tension was set to 10 N to minimize any wrinkling effects. The most effective advantage of gravure printing is high throughput. The Ag double-side seed layer of FPCB provides the highest increase in production rate (1–10 m/min printing speed) compared with other printing methods.

Printed patterns were sampled from the sheet using a slitting process for the drilled hole. The hole was drilled using a laser process, as shown in Fig. 5. The figure shows the printed front- and back-side views of the pattern; it was confirmed that the pattern was aligned to the exact position necessary. To prevent defects at the burned position, a burn was produced around the hole by the laser-drilling process, as shown in Fig. 5a, b. This process was needed in addition to the repair processes. The rand area was printed using an ink drop that compensated for such damage. The printed front- and back-side patterns had an average thickness of 1.42 and 1.86 μm at the A-A and B-B sections in Fig. 5a, b, respectively. The surface roughness of the Ag printed pattern showed average values of 520 and 700 nm (average uniformity 30 %) for the rough surface, and pin holes were observed, as shown in Fig. 6a, b. To investigate the surface morphology, the viscosity of Ag flake material should be decreased by tuning the amount of solvent. However, low-viscosity Ag flake material is not compatible as a seed layer for Cu plating. In this case, the printed thickness value is a more critical parameter that should be considered.

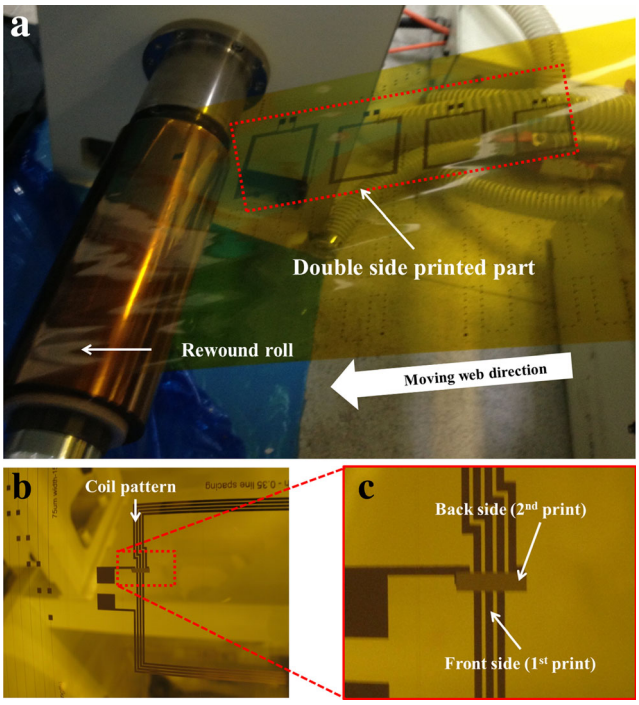

Fig. 4 Double-side printing process using R2R gravure technology: **a** photo of the R2R gravure printing system, **b** image of double-side printed circuits, and **c** detailed view of the front side (main circuit) and back side of the circuit

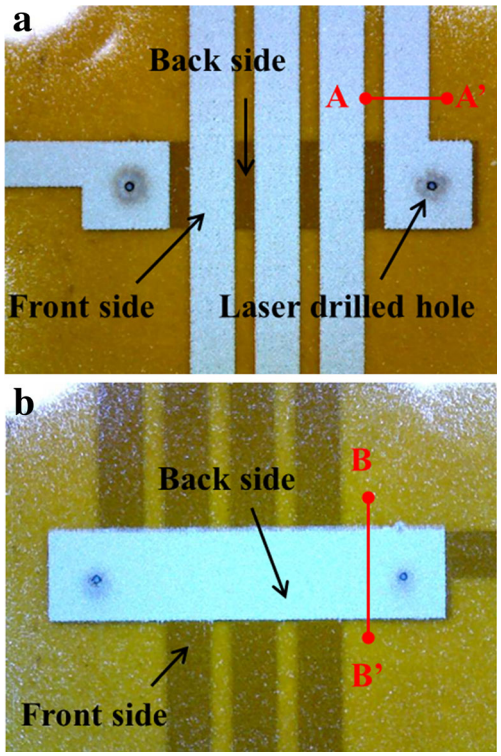

Fig. 5 Measurement of double-side printed patterns: images of **a** front side and **b** back side with laser-drilled holes on the terminals

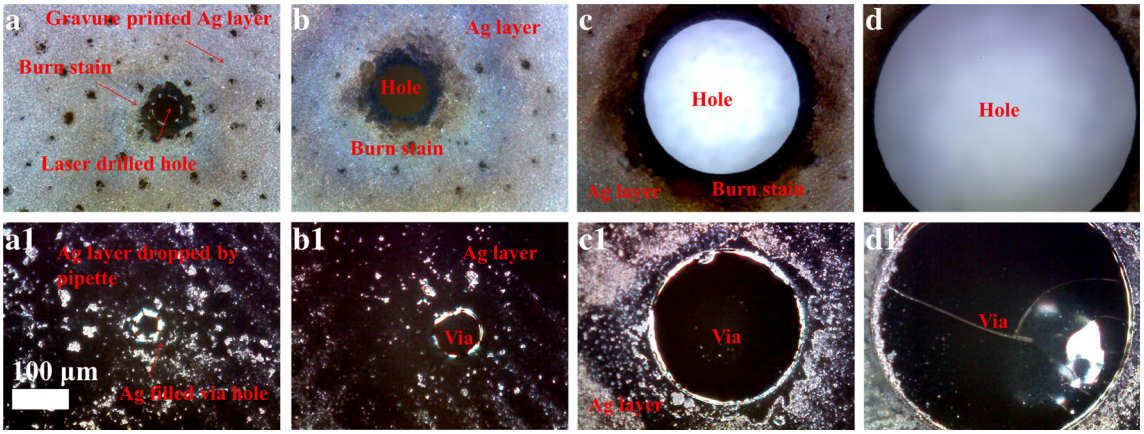

Fig. 6 Laser-drilled holes and ink filling by micropipettes: hole diameter of **a** 52 μm, **b** 97.6 μm, **c** 292 μm, and **d** 494 μm. **a1**–**d1** Images of the Ag-ink-filled holes

Figure 6 shows the results of the interconnection process. The laser-drilling performance shows excellent resolution below a 5 % standard deviation from the objective hole size. We assumed that there were electrical shortages and burrs surrounding the laser-drilled hole. To compensate for the expected damage, the filling process was carried out not only on the drilled hole surface but also around the hole-printed rand area. The clearance of the via filling occurred uniformly after the drying process. Ag ink drops were applied twice on each side of the substrate. After via-hole filling, the diameter of the hole was reduced. Ag ink covered the hole perfectly; however, the surface uniformity of the hole edges appeared rough. The hole edge roughness determines the interconnection performance; therefore, droplet control onto the via hole is a key aspect in producing a highly conductive circuit. In this experiment, the drop-casting method is sufficient for a hole diameter of 50 to 500 μm, but to prevent shortage between the adjacent patterns, small-droplet control is needed in the case of a fine-line pattern and/or narrow gap in the pattern. Inkjet printing technology could be a reasonable solution in this regard and may be adopted in further works. In addition, plating processes could be a suitable solution to improve the interconnection quality. Some parametric studies have already reported examples of interconnection improvements using Cu plating processes [39, 40].

Figure 7 shows the microscopic images and SEM images of the Ag-paste- and Cu-covered surface near with via hole. The Cu-plated coil pattern and via hole are present with good interconnection, as shown in Fig. 7a. The cross-sectional SEM image of section A-A in Fig. 7a indicates that the via wall consists of Ag–Cu layers and a Cu-covered rand area, as shown in Fig. 7b. The EDS profile indicates a large amount of Cu and Ag material on the via wall, as shown in the inset of Fig. 7b. Before the plating process, Ag flake particles were not cured perfectly by low-temperature curing, as shown in Fig. 7c. However, after Cu plating, the Cu particles cover the Ag flakes and fill the pores [30] between the Ag particles to afford good conductivity, as shown in Fig. 7d. The Ag flake pattern presents nonuniform surface distributions relative to the Cu-covered surface. This is also confirmed by AFM images as shown in Fig. 8. Figure 8a, b shows the Ag printed pattern and Cu-plated pattern on the Ag pattern, indicating the difference between each pattern. The average uniformity (roughness average: R_a) of each pattern near with edge was 140 and 76 nm, respectively, as shown in Fig. 8c. As a result, the Cu-covered pattern shows a good uniform surface and performs well in filling a rough surface with Cu.

The interconnection status and quality were identified by measuring the resistance of the printed circuit. Figure 9a shows the measurement method. The double-side printed circuit shown in Fig. 9a was measured from the start point to the end point of the coil pattern. The coil pattern had a width of 700 μm, line spacing of 300 μm, and line length of 1017.1 mm. As shown in the inset of Fig. 9a, the measurement point before the via hole (measurement points 1 to 2) and after the via hole (measurement points 1 to 3) suggests that the interconnection performance was sufficient. This was confirmed by applying an electric current to the printed board. Table 4 shows the results of the resistance measurement using a multimeter. The line resistances (measurement points 1 to 2) of the 1017.1-mm-long coil pattern with four types of holes were measured. For 0.05-, 0.1-, 0.3-, and 0.5-mm hole sizes, there were only minor changes in resistance (10, 21, 14, and 10 Ω, respectively) before and after via filling. The distance between measurement points 2 and 3 is approximately 21.05 mm. These small differences in resistance indicate a successful interconnection. This phenomenon is caused by the filling effect of the capillary force at the surface of the via hole. This observed effect does not seem to be correlated with the size of the hole. However, the results verify the performance of the interconnection for every case. After Cu plating of this pattern, the resistance rapidly decreased. Moreover, the difference before and after the via filling is 1–75 mΩ.

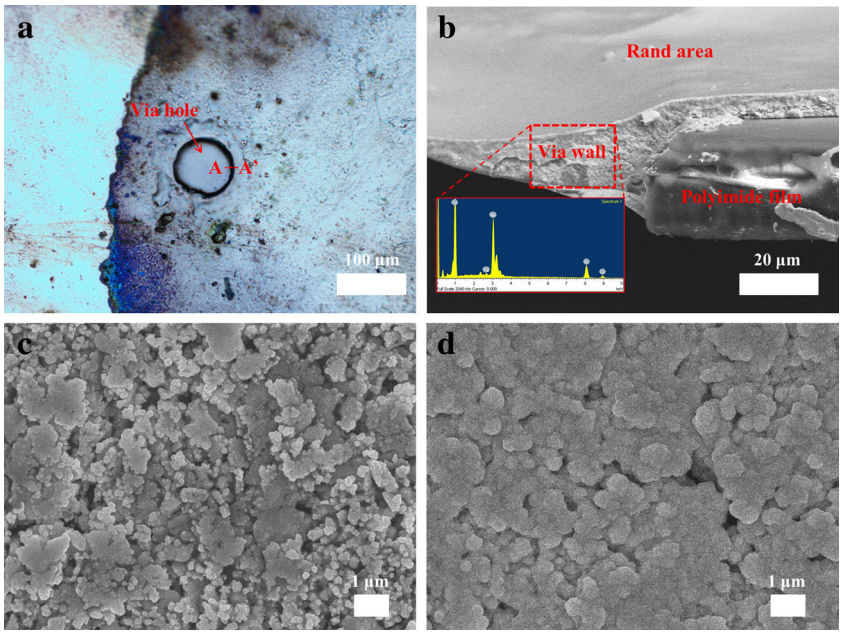

Fig. 7 **a** Microscopic image near via hole and **b** cross-sectional SEM image on A-A , indicating via wall and rand area (*inset*: EDS result on via wall). SEM images of **c** top surface of printed pattern by Ag flake paste and **d** plated Cu surface

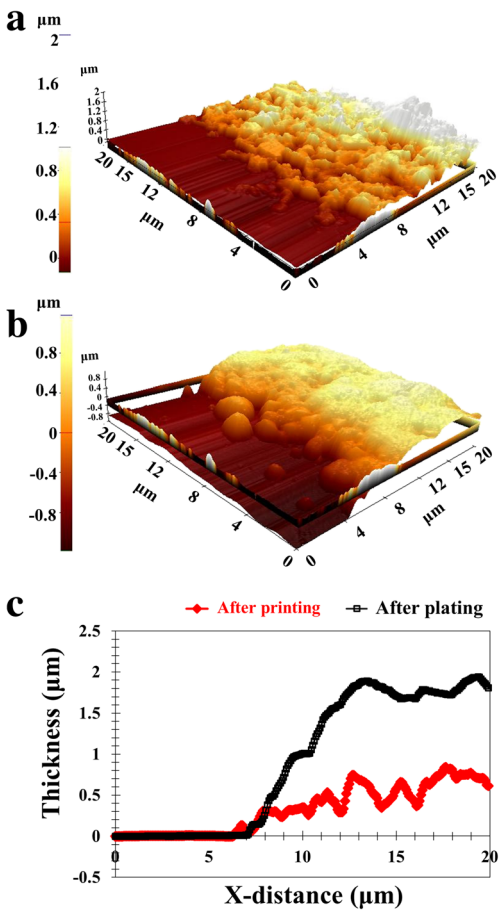

Fig. 8 Comparison of AFM images of **a** Ag printed layer and **b** Cu-plated layer on Ag layer. **c** Thickness profile of **a** and **b**

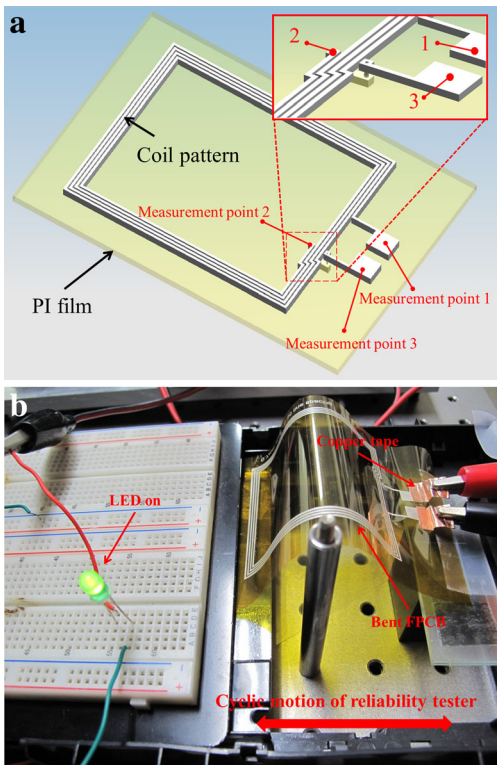

Fig. 9 Measurement of electrical resistance: **a** schematic of circuit (700-μm width, 300-μm line-spaced coil pattern) that shows measuring points (*inset* shows detail of the interconnected circuit between front and back side patterns) and **b** reliability test of double-side FPCB: cyclic bending experimental setup with LED for demonstrating electrical connection

Table 4 Measured line resistance according to the measurement points for various via-hole diameters

Diameter of via hole (μm)	Resistance value (kΩ)			
	Printed pattern		Cu-plated pattern	
	1 to 2	1 to 3	1 to 2	1 to 3
0.05	1.307	1.317	0.084	0.090
0.1	1.746	1.767	0.023	0.027
0.3	1.722	1.736	0.032	0.039
0.5	1.823	1.833	0.020	0.021

The final product of the via-filling process was set on a reliability tester. A voltage was applied for lighting the light-emitting diode (LED), as shown in Fig. 9b. A mass-produced FPCB is always subject to cyclic load when it is used for flexible applications. Therefore, the electrical characteristics were measured under a cyclic bending motion in real time for 400,000 cycles with a frequency of 1 Hz as listed in Table 5. Many resistance values were sampled. The average and standard deviation values of R/R_0 (R: measured resistance in bending cycles; R_0: initial resistance) within the bending cycles are presented for each of the four sections of bending cycles. To check the mechanical stability of each part of the device, a bending test was conducted twice at different positions (near the coil pattern and the via hole, with a bending radius of 5 and 12 mm, respectively). The bending radius in the via-hole case was smaller than that in the coil pattern case. The results show that the FPCB maintained steady electrical properties except for sampled overshoots (standard deviation). The doctor blading method, which is a type of screen printing using an Ag flake pattern, was compared with the fabricated FPCB. The doctor blading pattern shows a thickness over 10 μm that causes a high bending stress and an increase in resistance that was 1.5 times higher before 1000 cycles. It delaminated after 2000 cycles. It was proven that gravure printing of a seed layer was more stable than screen printing the layer because of its lower thickness and because of the nip and heating process on various rollers in the R2R system (calendering effect). Furthermore, the LED turned on at the start and the end points of the bending test. It was verified that the gravure-printed coil pattern, drop-cast via hole, and copper layer have good durability.

Additionally, the fabricated FPCB was tested in a 13.56-MHz RFID antenna application. The resonance frequency of the FPCB was 14 MHz and was confirmed by a higher value of peak-to-peak voltage, as shown in Table 6. The theoretical value of 12 MHz, calculated by equation $f=1/[2\pi\times sqrt(LC)]$, confirmed the similarity, where f, L, and C represent the resonant frequency, inductance, and capacitance, respectively (inductance of 0.8 μH was measured in the coil pattern, and a 222-pF commercial capacitor was used in the circuit).

4 Conclusions

In this study, we demonstrated a FPCB fabrication process that included gravure printing, drop-cast printing, and Cu plating. This was called a hybrid process. We introduced a new double-side printing logic using an R2R gravure process and verified its effectiveness. We performed experiments using the R2R large-scale mass production system and demonstrated that it could be applied in industry. Double-side printed patterns were fabricated on a PI film, and an Ag conductive paste was used. A continuously wound roll was sampled using a slitting procedure, and the sampled sheet was drilled by a laser. Drilled double-side patterns filled with low-viscosity Ag ink were used to form an interconnection between the front- and the back-side patterns. An ink drop method that used micropipettes for via-hole filling was adopted.

Table 5 Bending test result of each case

Case	Number of bending cycles (section)	Average value within cycles (R/R_0)	Standard deviation within cycles (R/R_0)
Bending on coil pattern	1 to 85,916	1.01	0.07
	85,917 to 171,833	1.00	0.02
	171,834 to 257,748	1.01	0.04
	257,749 to 393,664	1.00	0.01
Bending on via hole	1 to 81,437	1.11	0.37
	81,438 to 162,875	1.02	0.10
	162,876 to 244,312	1.01	0.03
	244,313 to 325,750	1.02	0.13
Doctor blading	1 to 4834	1.35	0.11
	4835 to 9668	1.46	0.04
	9669 to 14,502	1.38	0.03
	14,503 to 19,336	1.39	0.04

Table 6 Resonance frequency measurement result of the fabricated FPCB

Frequency (MHz)	V_{pp} (V)	Frequency (MHz)	V_{pp} (V)	Frequency (MHz)	V_{pp} (V)
1	102	18	120	35	41.5
2	105	19	74	36	38.6
3	106	20	86	37	36.3
4	110	21	114	38	34.2
5	113	22	118	39	32.6
6	118	23	110	40	30.7
7	122	24	98	41	29.2
8	130	25	86	42	27.3
9	138	26	80	43	25.3
10	150	27	74	44	24
11	162	28	68	45	23.2
12	178	29	64	46	22.6
13	192	30	60	47	21.7
14	198	31	50	48	20.3
15	188	32	56	49	19.7
16	130	33	46.9	50	19
17	122	34	44		

The final coil-patterned product was measured using optical and electrical devices. The resistance of the interconnected part showed few differences relative to its properties before via-filling and Cu plating process. To check for mechanical stability, a reliability test was conducted using a cyclic motion tester. The FPCB shows good electrical properties at 400,000 cycles. In addition, the fabricated FPCB was demonstrated as an RFID antenna. For this demonstration, the FPCB confirmed a 14-MHz resonance frequency that was close to the 13.56-MHz standard value. In further studies, we will attempt to improve the interconnection performance by adopting an online Cu plating process and inkjet filling that uses microdroplets. This could be called an online hybrid process. Moreover, complex structures and commercial target applications could be attempted using this fabrication logic. By using this advanced process, after developing a Cu solution material for the plateless process, we will be able to integrate all future process improvements and perform R2R gravure printing and via-filling processes continuously with good electrical performance.

Acknowledgments This work was supported by the Global Leading Technology Program funded by the Ministry of Trade, Industry and Energy, Republic of Korea (10042537), and by the Leading Foreign Research Institute Recruitment Program through the National Research Foundation of Korea (NRF) funded by the Ministry of Science, ICT & Future Planning (MSIP) (grant number: 2010-00525).

References

1. Cantatore E (2012) Applications of organic and printed electronics: a technology-enabled revolution. Springer
2. Keränen K, Korhonen P, Rekilä J, Tapaninen O, Happonen T, Makkonen P, Rönkä K (2015) Roll-to-roll printed and assembled large area LED lighting element. Int J Adv Manuf Technol:1–8. doi:10.1007/s00170-015-7244-6
3. Noh J-H, Kim I, Park S, Jo J, Kim D, Lee T-M (2013) A study on the enhancement of printing location accuracy in a roll-to-roll gravure offset printing system. Int J Adv Manuf Technol 68(5–8): 1147–1153. doi:10.1007/s00170-013-4907-z
4. Tseng H-Y, Subramanian V (2011) All inkjet-printed, fully self-aligned transistors for low-cost circuit applications. Org Electron 12(2):249–256. doi:10.1016/j.orgel.2010.11.013
5. Soltman D, Subramanian V (2008) Inkjet-printed line morphologies and temperature control of the coffee ring effect. Langmuir 24(5):2224–2231. doi:10.1021/la7026847
6. Cook BS, Cooper JR, Tentzeris MM (2013) Multi-layer RF capacitors on flexible substrates utilizing inkjet printed dielectric polymers. IEEE Microwave Wirel Compon Lett 23(7):353–355. doi:10.1109/lmwc.2013.2264658
7. Koski K, Koski E, Virtanen J, Björninen T, Sydänheimo L, Ukkonen L, Elsherbeni A (2012) Inkjet-printed passive UHF RFID tags: review and performance evaluation. Int J Adv Manuf Technol 62(1–4):167–182. doi:10.1007/s00170-011-3782-8
8. Dungchai W, Chailapakul O, Henry CS (2011) A low-cost, simple, and rapid fabrication method for paper-based microfluidics using wax screen-printing. Analyst 136(1):77–82. doi:10.1039/c0an00406e
9. Yang W, Russel T, Kai Y, Steve B, John T (2013) Screen printing of a capacitive cantilever-based motion sensor on fabric using a novel sacrificial layer process for smart fabric applications. Meas Sci Technol 24(7):075104
10. Shi CWP, Shan X, Tarapata G, Jachowicz R, Weremczuk J, Hui HT (2011) Fabrication of wireless sensors on flexible film using screen printing and via filling. Microsyst Technol 17(4):661–667. doi:10.1007/s00542-010-1161-2
11. Krebs FC, Fyenbo J, Jorgensen M (2010) Product integration of compact roll-to-roll processed polymer solar cell modules: methods and manufacture using flexographic printing, slot-die coating and rotary screen printing. J Mater Chem 20(41):8994–9001. doi:10.1039/c0jm01178a

12. Alstrup J, Jørgensen M, Medford AJ, Krebs FC (2010) Ultra fast and parsimonious materials screening for polymer solar cells using differentially pumped slot-die coating. ACS Appl Mater Interfaces 2(10):2819–2827. doi:10.1021/am100505e
13. Krebs FC (2009) Polymer solar cell modules prepared using roll-to-roll methods: knife-over-edge coating, slot-die coating and screen printing. Sol Energy Mater Sol Cells 93(4):465–475. doi:10.1016/j.solmat.2008.12.012
14. Park J, Shin K, Lee C (2014) Optimized design for anti-reflection coating process in roll-to-roll slot-die coating system. Robot Comput Integr Manuf 30(5):432–441
15. Kitsomboonloha R, Morris SJS, Rong X, Subramanian V (2012) Femtoliter-scale patterning by high-speed, highly scaled inverse gravure printing. Langmuir 28(48):16711–16723. doi:10.1021/la3037132
16. Yang J, Vak D, Clark N, Subbiah J, Wong WWH, Jones DJ, Watkins SE, Wilson G (2013) Organic photovoltaic modules fabricated by an industrial gravure printing proofer. Sol Energy Mater Sol Cells 109(0):47–55. doi:10.1016/j.solmat.2012.10.018
17. Hernandez-Sosa G, Bornemann N, Ringle I, Agari M, Dörsam E, Mechau N, Lemmer U (2013) Rheological and drying considerations for uniformly gravure-printed layers: towards large-area flexible organic light-emitting diodes. Adv Funct Mater 23(25):3164–3171. doi:10.1002/adfm.201202862
18. Noh J, Jung K, Kim J, Kim S, Cho S, Cho G (2012) Fully gravure-printed flexible full adder using SWNT-based TFTs. IEEE Electron Device Lett 33(11):1574–1576. doi:10.1109/led.2012.2214757
19. Lee C, Kang H, Kim C, Shin K (2010) A novel method to guarantee the specified thickness and surface roughness of the roll-to-roll printed patterns using the tension of a moving substrate. J Microelectromech Syst 19(5):1243–1253. doi:10.1109/jmems.2010.2067194
20. Nguyen H-A-D, Lee C, Shin K-H (2013) A mathematical model to predict surface roughness and pattern thickness in roll-to-roll gravure printed electronics. Robot Comput Integr Manuf 29(4):26–32. doi:10.1016/j.rcim.2012.10.003
21. Nguyen HAD, Lee J, Kim CH, Shin K-H, Lee D (2013) An approach for controlling printed line-width in high resolution roll-to-roll gravure printing. J Micromech Microeng 23(9):095010
22. Park J, Nguyen HAD, Park S, Lee J, Kim B, Lee D (2015) Roll-to-roll gravure printed silver patterns to guarantee printability and functionality for mass production. Current Applied Physics
23. Kawase T, Sirringhaus H, Friend RH, Shimoda T (2001) Inkjet printed via-hole interconnections and resistors for all-polymer transistor circuits. Adv Mater 13(21):1601–1605. doi:10.1002/1521-4095(200111)13:21<1601::aid-adma1601>3.0.co;2-x
24. Mandamparambil R, Fledderus H, van den Brand J, Saalmink M, Kusters R, Podprocky T, Van Steenberge G, De Baets J, Dietzel A A comparative study of via drilling and scribing on PEN and PET substrates for flexible electronic applications using excimer and Nd:YAG laser sources. In: Flexible Electronics & Displays Conference and Exhibition, 2009, 2–5 Feb. 2009 2009. pp 1–7. doi:10.1109/fedc.2009.5069273
25. Moscicki A, Falat T, Smolarek A, Kinart A, Felba J, Borecki J Interconnection process by ink jet printing method. In: Nanotechnology (IEEE-NANO), 2012 12th IEEE Conference on, 20–23 Aug. 2012 2012. pp 1–5. doi:10.1109/nano.2012.6322108
26. Koskinen S, Pykari L, Mantysalo M (2013) Electrical performance characterization of an inkjet-printed flexible circuit in a mobile application. IEEE Trans Compon Packag Manuf Technol 3(9):1604–1610. doi:10.1109/tcpmt.2013.2261774
27. Sridhar A, Cauwe M, Fledderus H, Kusters RHL, van den Brand J Novel interconnect methodologies for ultra-thin chips on foils. In: Electronic Components and Technology Conference (ECTC), 2012 I.E. 62nd, May 29 2012-June 1 2012 2012. pp 238–244. doi:10.1109/ectc.2012.6248834
28. Kang H, Baumann RR (2014) Mathematical modeling and simulations for machine directional register in hybrid roll-to-roll printing systems. Int J Precis Eng Manuf 15(10):2109–2116
29. Chang Y, Yang C, Zheng X-Y, Wang D-Y, Yang Z-G (2014) Fabrication of copper patterns on flexible substrate by patterning–adsorption–plating process. ACS Appl Mater Interfaces 6(2):768–772
30. Kang H, Sowade E, Baumann RR (2014) Direct intense pulsed light sintering of inkjet-printed copper oxide layers within six milliseconds. ACS Appl Mater Interfaces 6(3):1682–1687
31. Nguyen HAD, Lee J, Kim CH, Shin K-H, Lee D (2013) An approach for controlling printed line-width in high resolution roll-to-roll gravure printing. J Micromech Microeng 23(9):095010
32. Halonen E, Halme A, Karinsalo T, Iso-Ketola P, Mantysalo M, Makinen R Dynamic bending test analysis of inkjet-printed conductors on flexible substrates. In: Electronic Components and Technology Conference (ECTC), 2012 I.E. 62nd, May 29 2012-June 1 2012 2012. pp 80–85. doi:10.1109/ectc.2012.6248810
33. Quintero JAQ, Mancosu RD, De Oliveira AWC, Rolim DC, Da Silva OC, Silva JM Electro-mechanical evaluation of Ag trace patterns by ink-jet printing. In: Electronics Packaging Technology Conference, 2009. EPTC '09. 11th, 9–11 Dec. 2009 2009. pp 1000–1005. doi:10.1109/eptc.2009.5416397
34. Jakubowska M, Słoma M, Młożniak A (2011) Printed transparent electrodes containing carbon nanotubes for elastic circuits applications with enhanced electrical durability under severe conditions. Mater Sci Eng B 176(4):358–362. doi:10.1016/j.mseb.2010.10.002
35. Lee HM, Lee HB, Jung DS, Yun J-Y, Ko SH, Park SB (2012) Solution processed aluminum paper for flexible electronics. Langmuir 28(36):13127–13135. doi:10.1021/la302479x
36. Merilampi S, Laine-Ma T, Ruuskanen P (2009) The characterization of electrically conductive silver ink patterns on flexible substrates. Microelectron Reliab 49(7):782–790. doi:10.1016/j.microrel.2009.04.004
37. Nguyen HAD, Hoang N, Shin K-H, Lee S (2013) Statistical analysis on the effect of calendering process parameters on the geometry and conductivity of printed patterns. Robot Comput Integr Manuf 29(2):424–430
38. Lee C, Shin KH (2005) Strip tension control considering the temperature change in Multi-Span systems. J Mech Sci Technol 19(4):958–967. doi:10.1007/bf02919178
39. Krug K, Liu Y-F, Ho W-H, Lee Y-L, Dow W-P, Yau S-L (2012) Electrochemical Cu growth on MPS-modified Au(111) electrodes. J Phys Chem C 116(33):17507–17517. doi:10.1021/jp302406e
40. Kobayashi T, Kawasaki J, Mihara K, Honma H (2001) Via-filling using electroplating for build-up PCBs. Electrochim Acta 47(1–2):85–89. doi:10.1016/S0013-4686(01)00592-8